

Article

Evolutionary Trajectories of Coastal Sand Barriers along the West Portuguese Coast during the Holocene

Susana Costas 

Centre for Marine and Environmental Research (CIMA), University of Algarve, 8005-139 Faro, Portugal; scotero@ualg.pt

Abstract: Coastal sand barriers are dynamic features with complex depositional sequences holding critical information regarding system response to disturbances at secular to millennial time scales. Here, the evolutionary trajectories of three barriers located along the Portuguese coast are reconstructed over the Middle to Late Holocene using geophysical subsurface images, modern morphology and dating of dune and beach deposits. The integration of new and available information from the documents of the selected site contrasts histories with modern barriers displaying ages ranging from hundreds to thousands of years and non-linear trajectories defined by shifts between morphological states. Younger barriers appear to represent the latest progradational state within a history of landward barrier migration, where progradational states alternated with transgressive states. Conversely, the oldest barrier shows a single phase of barrier growth, despite some minor hiatus in progradation. Barrier state shifts appear to have simultaneously occurred across systems, suggesting external drivers of regional scale linked to Holocene climate variability, namely, periods of storminess activity, while the different trajectories displayed by the three sites appear related to site-specific variables controlling exposure to waves and winds. Exposed sites showed a lower ability to absorb disturbances and a greater range of system responses, varying between transgressive and progradational states.

Keywords: morphological states; transgressive coastal barrier; progradational coastal barrier; transgressive dune field; blowouts; foredune; ground penetrating radar; optical stimulating luminescence



Citation: Costas, S. Evolutionary Trajectories of Coastal Sand Barriers along the West Portuguese Coast during the Holocene. *J. Mar. Sci. Eng.* **2022**, *10*, 1894. <https://doi.org/10.3390/jmse10121894>

Academic Editor: Jorge Guillén

Received: 9 November 2022

Accepted: 1 December 2022

Published: 5 December 2022

Publisher's Note: MDPI stays neutral with regard to jurisdictional claims in published maps and institutional affiliations.



Copyright: © 2022 by the author. Licensee MDPI, Basel, Switzerland. This article is an open access article distributed under the terms and conditions of the Creative Commons Attribution (CC BY) license (<https://creativecommons.org/licenses/by/4.0/>).

1. Introduction

Coastal barriers comprise approximately 15% of the world's coastlines [1]. They are extremely dynamic and ephemeral features, mostly integrating a frontal beach, a dune or a set of dunes and backbarrier environments. As a result, coastal barriers may present complex depositional sequences that result from different combinations of environmental conditions, including sea-level history and simultaneously changing climate regimes occurring during the evolution of these systems. Depositional sequences can be categorised into two basic types: transgressive and regressive [2], resulting from contrasting modes of sedimentation. Each mode represents a distinctive balance between three fundamental forces controlling shoreface evolution; relative changes in sea level, rate of sediment input and rate of dissipation of wave and tidal energies [3]. Transgressive sequences are mainly associated with transgressive barriers formed during the Postglacial Marine Transgression, although they have also been formed after sea-level stabilisation at receding coastlines. Regressive sequences formed once the sea level reached a stable position ca. 6000–6500 years ago and can be associated with both prograding and stationary barrier types [3]. Transgressive and regressive barriers are not exclusive to a particular coastal stretch and may coexist within the same geological province and under uniform sea-level conditions as a result of differences in sediment supply, e.g., [4]. In addition, these systems may not follow linear trends, shifting between these two states over time as the sediment input and climate regimes oscillate. Absolutely stationary barriers probably do not exist,

even if they do not show a net trend [5], but they might show alternating transgressive and regressive behaviours [6].

The evolutionary trend of a particular coastal barrier may determine not only the stratigraphy of the barrier itself but also the nature of the associated coastal dunes. Psuty [7] proposed a conceptual model to explain the direct relationship between the sediment budget within a beach and the adjacent dune system. In general terms, shore-parallel foredune ridges are usually found in regressive barriers, while active transgressive dunes appear more frequently associated with retrograding barriers or barrier retrogradation phases (transgression). However, it is not clear yet how transgressive dune fields are initiated or maintained over time [8,9]. Suggested initiation mechanisms include climate change, sea-level oscillations, foredune destabilisation, shoreline erosion, disturbance or destruction of the vegetation cover, and the coalescence of parabolic dunes [9]. Many authors agree that coastal erosion, triggered by sea-level transgression, initiated late Pleistocene and Early to Middle Holocene transgressive dune fields [5,10–12]. At shorter temporal scales, transgressive dunes initiation was related to negative sediment budget within the beach system and subsequent destabilisation of the foredune [7] or regular destabilisation of the backshore/dune interface, allowing a higher landward sand transport during the action of strong onshore winds [5]. Alternatively, examples can be found arguing that transgressive dune fields can form as sea-level falls during regression as sediment-rich shelves become exposed to winds, e.g., [13]. Despite the initiation mechanism, transgressive dune fields migrate across- and alongshore, significantly cannibalising, modifying, and eliminating former dune fields [8].

The sandy coast of Portugal is dominated by large stretches of starved shorelines, showing average cross-shore change rates of -0.24 ± 0.01 m year⁻¹ [14], which is generating severe problems of land loss and infrastructures. These circumstances could imply favourable conditions for the initiation of transgressive dune fields. However, the rare occurrence of such active systems highlights the decisive role of other concurrent factors necessary to initiate transgression, for example, the prevalence of winds strong enough to mobilise sediment in these sandy coasts [15] and the volume of sediment available within the coastal plain or sediment stock. In turn, the record of aeolian activity through the Late Pleistocene and Middle to Late Holocene documents that the Portuguese coast was episodically inundated by aeolian sand sheets migrating inland [16].

The present study aims to reconstruct the evolution of sandy coastal barriers over the Middle to Late Holocene, building upon previous works carried out along the Portuguese coast and complementing the analysis with new data. For this purpose, different sources of information from three representative coastal segments distributed along the Portuguese coast are integrated in order to better understand patterns of response and evolution of sandy coasts through this period of time. Integrated information includes subsurface geophysical stratigraphy, the chronology of major units and the morphological characterisation of present features. Data from coastal barriers and adjacent, stabilized transgressive dune fields from two of the investigated sites have been published and partially discussed in previous works [16–18]. Here, a third coastal plain is explored and analysed in order to expand the spatial coverage of the analysis and to assess the validity of evolution patterns previously put forward. In this regard, this work will contribute to understanding the evolutionary trajectories of coastal barriers through the Middle to Late Holocene, the role of transgressive dunes within these paths, the drivers behind the observed changes, and to understand the implications to present-day situation and future evolution.

2. Explored Coastal Sectors

The sectors explored within this work meet a series of conditions that highlight their relevance at a regional scale. Among these are the dimensions of the coastal system, the presence of fixed transgressive dune fields inland of the present coastal plain, the storage of large volumes of sediment within the coastal plain and transgressive dune field, and the availability of information. From north to south, the selected sites comprise (i) an exposed

coast between Mira Beach and Cape Mondego (Segment A, Figure 1), (ii) a relatively exposed coastal area downdrift of the Tagus estuary mouth at the coastal plain of Costa da Caparica (Segment B, Figure 1), and (iii) a protected spit enclosing the Sado estuary (Troia Peninsula; Segment C, Figure 1). The three sites are located along the western mesotidal (i.e., 3.6 m maximum range during Spring tides on average) coast of Portugal. This coastal stretch is shaped by average wave heights that range between 2.2 m in the northern part (Figueira da Foz [19]) and 1.7 m in the southern part (Sines [19]) (Figure 1). In addition to the general southward decrease in the incident wave height, Segments B and C are partially protected from the northern waves, which are the more frequent waves approaching this coast (71 to 77% of the incident waves). Segment B is protected by the presence of Cape Raso, located to the north of the Tagus estuary mouth, while Cape Espichel shelters Segment C (Figure 1). The mean annual longshore sediment transport, estimated for the northern area and using hindcast waves for the period between 1953 and 2010, is around 1 million cubic meters directed to the south, showing an irregular and noncyclic pattern, with yearly averages ranging from 108,000 to 2.24 million $\text{m}^3 \text{ years}^{-1}$, always directed to the south [20]. As mentioned in the introduction section, the evolution of two of the three selected sites, namely Segments A and C, have been previously investigated and described in detail in [17,18,21], while the evolution of Segment B will be investigated in the present work.

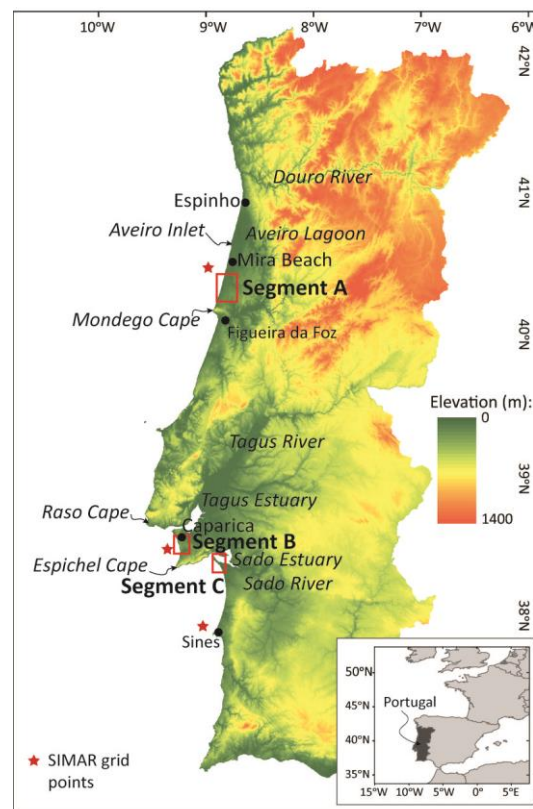


Figure 1. Location of the selected sites (Segments A to C) along the west coast of Portugal.

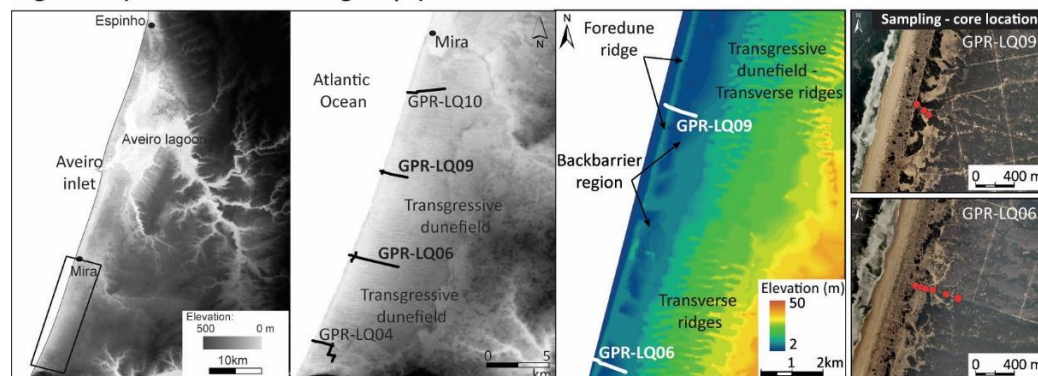
2.1. Coastal Segment A (Mira to Mondego Cape)

Segment A is part of the coastal stretch that extends between Espinho and Mondego Cape (Figure 1), enclosing the Aveiro Lagoon. The recent evolution of this coastal area is dominated by localised severe problems of erosion and shoreline retreat, namely downdrift the Aveiro inlet and initiated by its artificial fixation in 1808, with rates of around 8 m/year. Progradation has dominated shoreline trends downdrift Mira Beach over the past decades [22].

Recent investigations determined the age of the present coastal barrier and adjacent transgressive dunes to reconstruct the evolution of this coastal segment, suggesting a

complex evolution dominated by episodes of barrier formation and growth, alternating with episodes of barrier destruction [17]. The authors suggest that the modern coastal barrier, which is around 360 years old, represents the latest pulse of barrier elongation and lagoon enclosing, while identified units of transgressive dunes represent episodes of barrier transgression and dismantling occurring 4.25–3.32 and 1.14–1.04 ka ago (Figure 2). This interpretation is further supported by the occurrence of lagoon deposits dated around 4500 and 2000 ka [23,24], which imply the existence of former barriers during the Middle and Late Holocene.

Segment A (Mira Beach to Mondego Cape)



Reconstruction - facies architecture and ages

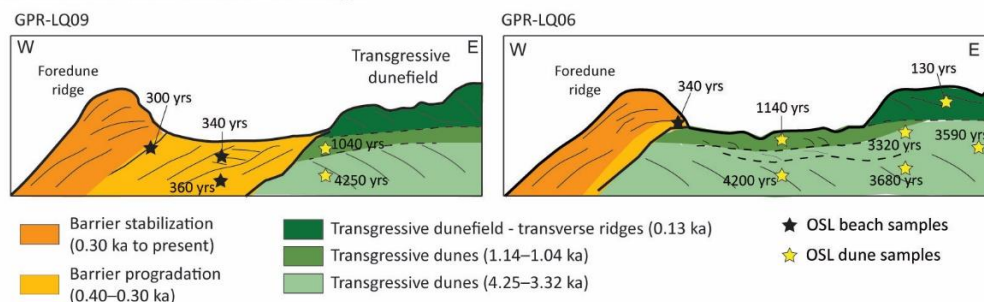


Figure 2. Detail of the location of the site Segment A, the morphology of the modern barrier and inland transverse ridges conforming to the fixed transgressive dune field and the reconstruction of the evolution of the area based on Costas et al. [17].

South of Mira, the barrier attaches to a transgressive dune field, consisting of transverse dunes, that extends landwards for 7 km (Figure 2). The most prominent aeolian features are 1 km long elongated ridges with a spacing of 200 m. The analysis of this transgressive dune field documents the occurrence of several pulses of aeolian activity over time, namely during the Younger Dryas [24] between 9.7 and 8.2 ka and during the Little Ice Age [25].

2.2. Coastal Segment B (Fonte da Telha to Caparica Coastal Plain)

Segment B is part of the coastal plain that extends between Trafaria and Cape Espichel, located to the south of the Tagus River mouth (Figures 1 and 3). The Caparica coastal plain is located at the toe of a cliff formed by Plio-Pleistocene sands [26]. The southern part of the coastal plain is characterised by a narrow beach at the toe of the cliff, with waves frequently affecting it. The coastal plain widens towards the north, increasing the distance to the cliff from 300 m at Fonte da Telha to about one kilometre at the vicinity of the estuary mouth (Figure 3), where the coastal barrier is separated from the cliff by a wetland currently occupied by agricultural activities.

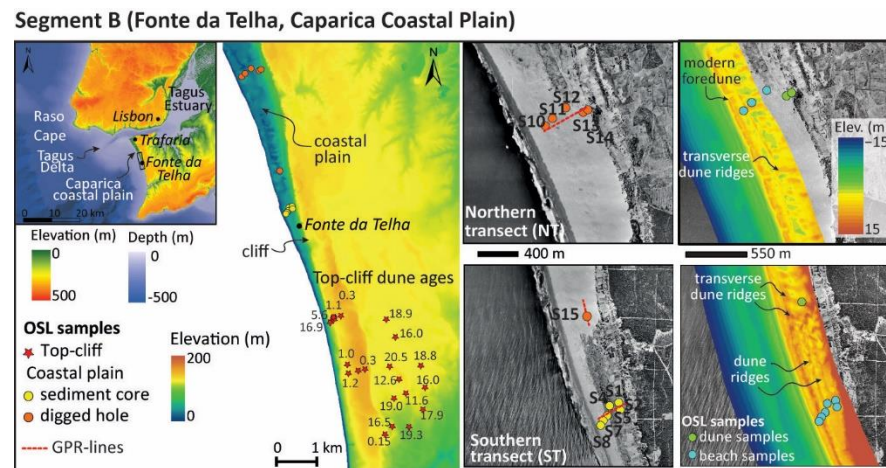


Figure 3. Detail of the location and morphology of Segment B, including the age of the top-cliff dunes based on [15,16] and the new sampling (for dating and geophysical image collection) carried out in the coastal plain.

At present, this coast is one of the main hotspots of erosion within the Portuguese coast related to the dredge activities of the Tagus navigational channel [14]. Human occupation is recent (i.e., by the end of the XVIII century, occupation was seasonal) and concentrates within the northern part of the coastal plain, originally oriented to fishery and agriculture purposes [27]. In 1830, the occupation of this area was legalized. Erosion problems only began when population density drastically increased, and the beach started to be used for leisure purposes.

The area where the present study focuses is located to the south of the heavily occupied area. The original landscape in this area has been slightly modified by human activities that include the building of a train for touristic purposes, the plantation of trees for dune fixation, the adaptation of areas for parking spaces, and the construction of restaurants within the foredune ridge. The latter is about 50 m in width and partially fragmented, with elevations around 10 m above MSL. In some areas of the coastal plain, this ridge appears backed by a series of dune ridges (Figure 3).

The formation of this coastal plain was associated with the Lisbon earthquake of 1755 [28]. The authors suggest that tectonic adjustments related to this event allowed the seaward displacement of the shoreline from the toe of the cliff, allowing the development of the coastal plain. Conversely, recent works hypothesised a more complex evolutionary history, sharing some similarities with Segment A, which includes the occurrence of several episodes of barrier dismantling and construction with the subsequent inland migration of transgressive dunes. The latter are currently found at the top of the cliff and have been dated and described in Costas et al. [16] (Figure 3). According to this research, the last pulse of transgressive dunes reaching the top of the cliff dates from about 1000 years ago; However, the age of the modern coastal barrier has yet to be determined as well as the proposed hypothesis of coastal evolution.

2.3. Coastal Segment C (Troia Peninsula)

Finally, coastal Segment C focuses on the Troia Peninsula, which represents the northern end of the 62 km long Troia-Sines littoral arc. This sandy peninsula is attached at its southern end to the mainland and extends for 24 km to the north, restricting the exchange of water between the estuary and the Atlantic Ocean to the Sado Inlet (Figures 1 and 4). The peninsula is located within the shadow zone generated by the Espichel Cape [29] and shows a very different and more continuous evolutionary history (Figure 4).

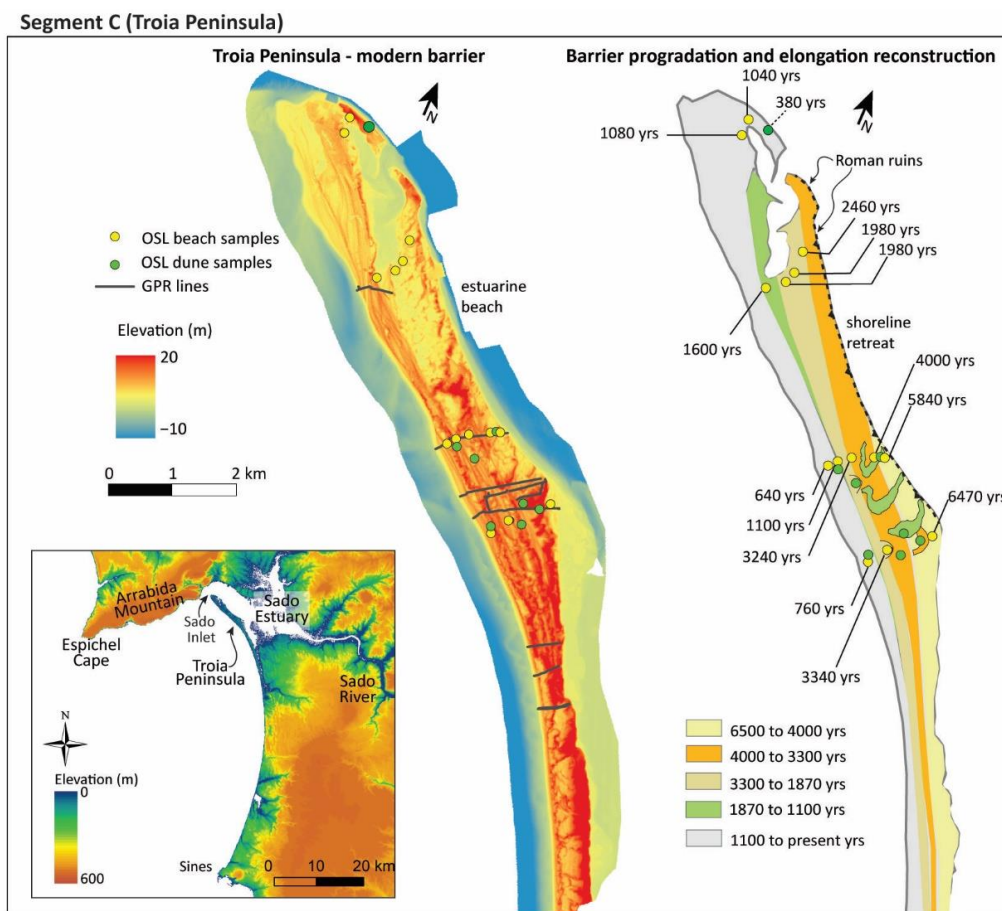


Figure 4. Detail of the location of Segment C and evolution over the Middle to Late Holocene based on Costas et al. [18].

The present state of the peninsula does not show clear signs of retreat apart from temporary erosive hotspots concentrated in the vicinity of its northern end that could be related to the short-term morphodynamics of the ebb-delta. In addition, frequent scarps reaching the foredune toe can be found along most of the peninsula. Most of the low occupation, represented by hotels and holiday houses, is presently concentrated at the end of the sandy peninsula. However, the presence of roman ruins within the estuarine margin of the spit reveals an earlier occupation that was linked to fishing and derived activities that were partially eroded by shoreline retreat within the estuarine beaches [18] (Figure 4). The abandonment of this occupation was coincident with the active migration of parabolic dunes moving seaward (i.e., from the estuarine margin towards the seaward margin of the spit) and dated around 1700 years ago [18]. The formation and growth of the Troia Peninsula were described in detail by Costas et al. [18,21] (Figure 4). The authors set the initiation of the spit about 6.5 ka ago after the sea-level rise rate attenuated. Following this, the spit started its elongation and progradation with the formation of five major dune ridges or sets that represent the growth of the peninsula through both seaward progradation and northward elongation [18].

3. Materials and Methods

The materials and methods used to investigate the evolution of the coastal plain in Segment B are described in detail in this section. The information on barrier evolution (i.e., stratigraphy and chronology) available from Segments A and C, which are detailed and presented in Costas et al. [17] and in Costas et al. [18,21], respectively, were compiled and compared with data from the coastal plain at Segment B. Comparison between sites was possible as the methodology applied at all sites followed the same procedures, which

comprised two main steps. The first step consisted of exploring the stratigraphy of the study sites, aiming at identifying the spatial distribution of beach and dune deposits within the coastal plains and the main aeolian units within the inland dune fields when present. Once the stratigraphy was defined, sediment samples were collected for dating and chronological determination of the identified stratigraphy.

The stratigraphy was explored with support to subsurface geophysical techniques, namely Ground Penetrating Radar (GPR), combined with subsurface sediment cores for groundtruthing. At Segment B, the geophysical data collected comprises a total of 1.5 km of cross-shore and longshore profiles within the coastal plain (Figure 3). Images of the subsurface were acquired using an Ingegneria Dei Sistemi-Ground Penetrating Radar (IDS-GPR) system RIS MF Hi-Mod #1 equipped with a dual frequency antenna (200 and 600 MHz). GPR was used to reconstruct the progradation and growth of the coastal plain by mapping subsurface scarps and accretionary units. Maximum penetration (depth around 6 m) was achieved using the 200 MHz antennae. Low penetrations were found at the vicinity of the beach, the toe of the cliff and below the water table due to the attenuation of the electromagnetic waves by the presence of saltwater infiltrations, clay minerals from the cliff and the high dielectric constant of water molecules, respectively [30]. The GPR was synchronized to an RTK-GPS system in order to obtain the topographical information for static correction during the processing of the radargrams. Raw data were processed using the program package Reflex-Win Version 5.0.5 by Sandmeier Software. Processing included time-zero drift, application of filters and gains, velocity profile estimate, migration and static corrections. An average subsurface velocity of 0.13 m/ns was estimated using the interactive hyperbola-adaptation method for dry sand, while velocities around 0.07 m/ns were found within wet sands.

Results from GPR were integrated with high-resolution digital terrain models from LiDAR (provided by the Direção-Geral do Território and surveyed in 2011) and aerial photographs (from the year 1958) to select the best locations for sample collection for dating. The method used to date when the beach was growing and the dunes were actively moving was optical stimulating luminescence (OSL). The samples were collected with support to a TESS-1 suction corer [31]. Six suction cores (4 m in length) of beach and dune sediments were collected along one cross-shore GPR line (Figure 3). The rest of the samples were collected within the surface layer by digging 1 m deep holes to avoid surface remobilization problems. Once at the surface, a segment of 35 cm centred at the desirable depth was cut off and sealed. The sections of the cores not used for dating were split for core description and sampling for macroscopical and textural analysis. All cores and surface samples were retrieved in dark grey and opaque PVC tubes to avoid exposure of sediments to sunlight, hence suitable for luminescence dating. The procedures applied for OSL dating were the same as in [15–17] and summarised below.

The samples were dated at the University of Nebraska-Lincoln's Luminescence Geochronology Laboratory. Sample preparation for Dose-Rate Determination was carried out under amber-light conditions. Samples were wet sieved to extract the 150–250 μm fraction and then treated with dilute HCl to remove carbonates. Quartz and feldspar grains were extracted by flotation using a 2.7 gm cm^{-3} sodium polytungstate solution, then treated for 60 min in 48% HF, followed by 30 min in 47% HCl. The sample was then resieved, and the <150 μm fraction was discarded to remove residual feldspar grains. The etched quartz grains were mounted on the innermost 2 or 5 mm of 1 cm aluminium disks using Silkospray. The dose rates were calculated using the method of Aitken [32] and Adamiec and Aitken [33], and dose-rate conversion factors were from Guerin et al. [34] and attenuation coefficients from Brennan [35]. The cosmic contribution to the dose rate was determined using the techniques of Prescott and Hutton [36].

OSL analyses were carried out on Riso Automated OSL Dating System Model TL/OSL-DA-15B/C and TL/OSL. The DA-20 readers were equipped with blue and infrared diodes using the Single Aliquot Regenerative Dose (SAR) technique [37]. All equivalent dose (D_e) values were determined using the Central Age Model [38] unless data analysis indicated

partial bleaching, in which case the Minimum Age Model [38] was used. Optical ages were based on a minimum of 50 aliquots [39]. Individual aliquots were monitored for insufficient count-rate, poor quality fits (large error in D_e), poor recycling ratio, strong medium vs. fast component [40] and detectable feldspar. Aliquots deemed unacceptable based on these criteria were discarded from the data set prior to averaging. Averaging was carried out using the Central Age Model [38] unless the D_e distribution (asymmetric distribution; skew $> 2 \sigma$, Bailey and Arnold [41]) indicated that the Minimum Age Model [38] was more appropriate instead.

The exposure to waves and winds of the three selected sites was qualitatively assessed (see Discussion Section 5.1) with support to deep water wave and wind conditions retrieved from the SIMAR database [42], which is a 58-year wave re-analysis freely distributed by Puertos del Estado (Spain). Local conditions were assessed using the closest SIMAR grid point to each of the coastal segments (Figure 1), covering the period between February 1958 and the present day.

4. Results

This section begins by presenting and describing the results from Segment B in terms of internal stratigraphy, dates and modern morphology, which will support the reconstruction of the evolution of this segment. Later, the evolution of the other two selected segments, investigated in previous works, will be integrated with the evolution from Segment B to elaborate on the morphologic states and evolutionary trajectories of the studied coastal barriers.

4.1. Coastal Segment B

4.1.1. Subaerial Morphology

The explored area can be divided into two sub-zones based on the morphology and type of dunes identified within the aerial photographs from 1958 and high-resolution topographic information derived from the available LiDAR dataset collected in 2011 (Figure 3). The first, located to the north, is characterised by the presence of mobile and unvegetated dunes covering the coastal plain. The dunes appear to migrate southward, forming 100 m wide and 4 m high transverse ridges. The mobile dunes were artificially fixed through the implementation of afforestation measures aiming at transforming the area into fertile lands to use for agricultural purposes [27]. The southern limit of this mobile dune field is characterised by small and isolated parabolic dunes migrating to the south. The topography shows how the migration of these features changed the landscape, erasing former foredune ridges, which appear to have been recycled and transformed into mobile dunes. The limit of the mobile dunes shows the contact with the former dune ridges. Four ridges can be identified, including the active one, which documents the progradation of the littoral arc in this zone. Southward of this zone, the toe of the cliff is very close to the shoreline, and the number of dune ridges is reduced to one that disappears south of Fonte da Telha (Figure 3).

4.1.2. Internal Stratigraphy

The same principles, applied by Costas et al. [17,18] and based on Mitchum et al. [43], were adopted here in order to facilitate the comparison between sites. In this line, the classification of the internal reflectors was primarily related to their continuity, attitude and interval, which allowed simplifying the internal variability identified within the GPR images into two facies associations, summarised in Table 1. A horizontal strong and discontinuous reflector running across the barrier at around 1.5 m above MSL is interpreted as the water table associated with a subsurface freshwater aquifer (Figure 5). Reflection-free areas within the radargrams are a consequence of signal attenuation due to the presence of saltwater intrusions from the beach, the presence of fine-grained sediments from the erosion of the cliff and the actual freshwater aquifer.

Table 1. Facies associations and characterisation of identified radar facies.

Facies	Radar Features	Interpretation
RF1-1	Low-amplitude, sub-horizontal reflectors	Constructional (aggradation) stages of the beach (berm welding)
RF1-2	Sigmoid-oblique reflections dipping seaward	Progradation seaward of the beach foreshore
RF2-1	Wavy concave down reflectors, frequently found overlaying RF1	Accumulation of sand blown from the adjacent beach trapped by vegetation
RF2-2	Sub-horizontal and tangential-oblique reflectors, slightly dipping seaward	Vertical aggradation of the backshore with reduced vegetation cover and frequent deflation surfaces
RF2-3	Tangential-oblique reflectors dipping seaward	Seaward advance of foredunes or accretion of foreslopes
RF2-4	Oblique parallel and tangential-oblique reflectors, most frequently dipping landward	Transverse ridges associated with the past mobile dunefield

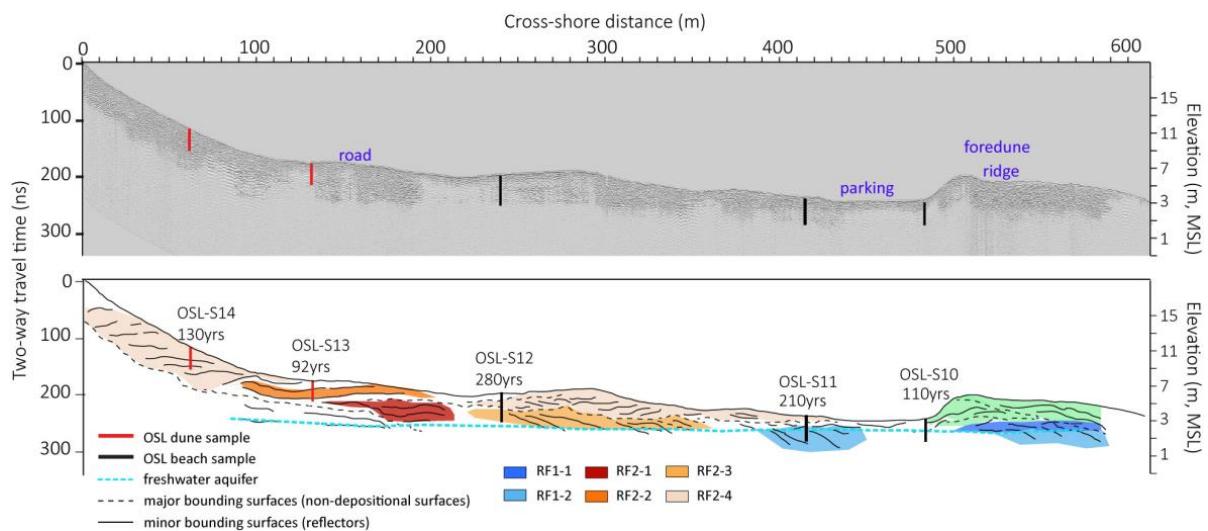


Figure 5. The upper panel shows the radargram corresponding to GPR-NT (i.e., northern transect in Figure 3) measured across the coastal plain at Fonte da Telha. The lower panel presents the interpretation of the radargram showing identified radar facies, the position of the sediment samples for dating and their ages.

The first facies association consists of low-amplitude sub-horizontal reflectors (facies RF1-1) and sigmoid-oblique reflections dipping seaward (facies RF1-2) that can be found overlaying, crossing and underlying the water table (Figures 5 and 6). Their location, relative to the MSL, suggests that marine processes may be important to their accumulation. However, the different configurations also suggest that both RF1 facies may represent different depositional processes within the upper beach. In the first case (RF1-1), they can be associated with constructional (aggradation) stages of the beach through beach berm welding, while the second (RF1-2), being represented by reflectors with similar slopes to the present beach foreshore, can be associated with the seaward progradation of this zone of the beach. Van Heteren et al. [44,45] associated these complex sigmoid-oblique configurations with periods of alternating aggradation and progradation linked to beach recovery processes.

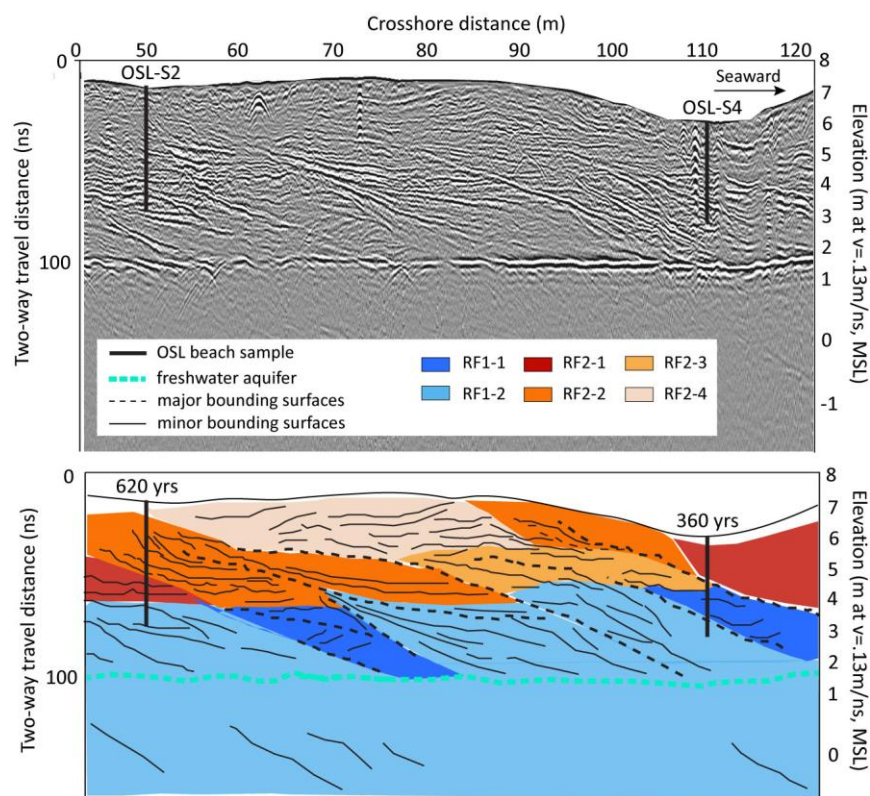


Figure 6. The upper panel shows part of the radargram corresponding to GPR-ST (i.e., southern transect in Figure 3) measured across the coastal plain at Fonte da Telha. The lower panel presents the interpretation of the radargram showing identified radar facies and the position of the sediment samples for dating and their ages.

The second facies association overlays RF1 (i.e., the upper beach sediments) across and along the explored coastal barrier (Figure 5). The association of facies includes facies RF2-1, which is characterised by wavy concave down reflectors that are frequently found overlaying RF1 deposits. This facies is interpreted as representing the accumulation of sand blown from the adjacent beach trapped by vegetation. High-amplitude sub-horizontal and tangential-oblique reflectors, slightly dipping seaward, feature RF2-2 and usually overlay facies RF1-1. Facies RF2-2 represent the vertical aggradation of the backshore through the accumulation of blown sand with reduced vegetation coverage and frequent deflation surfaces. Tangential-oblique reflectors (facies RF2-3) dipping seaward can be identified directly overlying RF1, RF2-1 and RF2-2. They represent the seaward advance of foredunes, promoting the progradation of the dune following beach progradation. Finally, facies RF2-4 is represented by oblique parallel and tangential-oblique reflectors most frequently dipping landward and with frequent erosional upper toplap terminations. These facies were identified in the sectors of the GPR lines running across the transverse ridges associated with the past mobile dune field. RF2-4 represents the upper part of the stratigraphy within the northern explored zone and its reflectors downlap onto erosive or non-depositional bounding surfaces that truncate other RF2 facies (Figure 5).

4.1.3. Chronology

The results of the optically dated samples collected within the dune (two samples) and the beach (ten samples) deposits and along two transects running across the coastal barrier are summarised in Table 2 (see Figure 3 for location). The dune samples were collected within the area where the transverse ridges associated with the mobile dune field were identified (Figure 3). The OSL ages are presented in years before the sampling, as referred to in the sample name (i.e., 2011 or 2013).

Table 2. Luminescence dating results. OSL ages are represented in years before 2011 or 2013, depending on the collection date specified in the sample name (second column). Shaded rows represent samples collected within the dune, while white rows show the results for the beach sediment samples.

UNL#	SAMPLE	Burial Depth (m)	Cosmic (Gy)	Dose Rate (Gy/ka)	D _e (Gy)	Aliquots	Age (ka)
UNL3403	S1-2011	3.86	0.12	1.44 ± 0.05	0.89 ± 0.08	53	0.62 ± 0.06
	Minimum Age Model [38]				0.50 ± 0.02		0.35 ± 0.02
UNL3404	S2-2011	4.65	0.11	1.18 ± 0.05	0.73 ± 0.03	50	0.62 ± 0.03
UNL3492	S4-2011	2.0	0.16	1.33 ± 0.05	0.48 ± 0.04	53	0.36 ± 0.03
UNL3493	S5-2011	2.1	0.16	1.36 ± 0.05	0.25 ± 0.02	57	0.19 ± 0.02
UNL3494	S7-2011	1.9	0.16	2.08 ± 0.07	0.36 ± 0.03	55	0.17 ± 0.02
UNL3495	S8-2011	1.9	0.16	1.83 ± 0.06	0.21 ± 0.01	50	0.11 ± 0.01
UNL3694	S10-2013	1.2	0.18	1.85 ± 0.07	0.21 ± 0.01	55	0.11 ± 0.01
UNL3695	S11-2013	1.1	0.18	1.65 ± 0.08	0.34 ± 0.01	64	0.21 ± 0.01
	Minimum Age Model [38]				0.30 ± 0.01		0.18 ± 0.01
UNL3696	S12-2013	0.8	0.19	1.53 ± 0.06	0.42 ± 0.02	53	0.28 ± 0.02
	Minimum Age Model [38]				0.35 ± 0.13		0.23 ± 0.08
UNL3697	S13-2013	1.15	0.18	1.72 ± 0.07	0.16 ± 0.01	59	0.092 ± 0.009
	Minimum Age Model [38]				0.15 ± 0.01		0.085 ± 0.008
UNL3698	S14-2013	0.85	0.19	1.77 ± 0.09	0.24 ± 0.02	55	0.13 ± 0.01
UNL3699	S15-2013	0.80	0.19	1.79 ± 0.07	0.19 ± 0.02	57	0.11 ± 0.01
	Minimum Age Model [38]				0.14 ± 0.02		0.076 ± 0.009

The range of obtained ages for the beach sediments varies between 110 and 620 years. The oldest ages were collected within the southern transect (Figures 6 and 7b) at the toe of the cliff. Seaward from this location, the age of the beach sediments decreases, documenting the gradual progradation of the sandy coastal barrier. A similar trend was observed in the northern transect (Figures 5 and 7b), whose oldest obtained age was yielded at 230 years. The latter was located about 100 m seaward of the toe of the cliff because the landward-most beach sediments identified within the GPR line were inaccessible. The youngest beach samples were collected within the landward part of the current foredune, depicting the age when it started to develop and grow. This also suggests that these samples may also be informative about the moment when beach progradation stopped and the shoreline became stable, promoting the growth of the foredune.

In general terms, the age results from both transects document very different progradation rates alongshore and within each transect over time. The average progradation rate estimated for transect NT (297 m long) was 2.48 m/year, while the maximum rate within the transect reached 3.64 m/year, between 230 and 180 years ago, dropping to 1.64 m/year over the second time interval (i.e., from 180 to 110 years ago). The average progradation rate estimated for transect ST (211 m long) was 0.41 m/year, with partial rates ranging from 2.4 m/year (between 190 and 170 years ago) to 0.26 m/year (between 360 and 190 years ago). The period 190–170 is comparable to the interval within transect NT when maximum progradation rates were recorded (i.e., a period from 230–180 years ago), suggesting a

period with boosted progradation rates between 230 and 170 years ago. The progradation rate between 170 and 110 years ago in ST was 0.65 m/year.

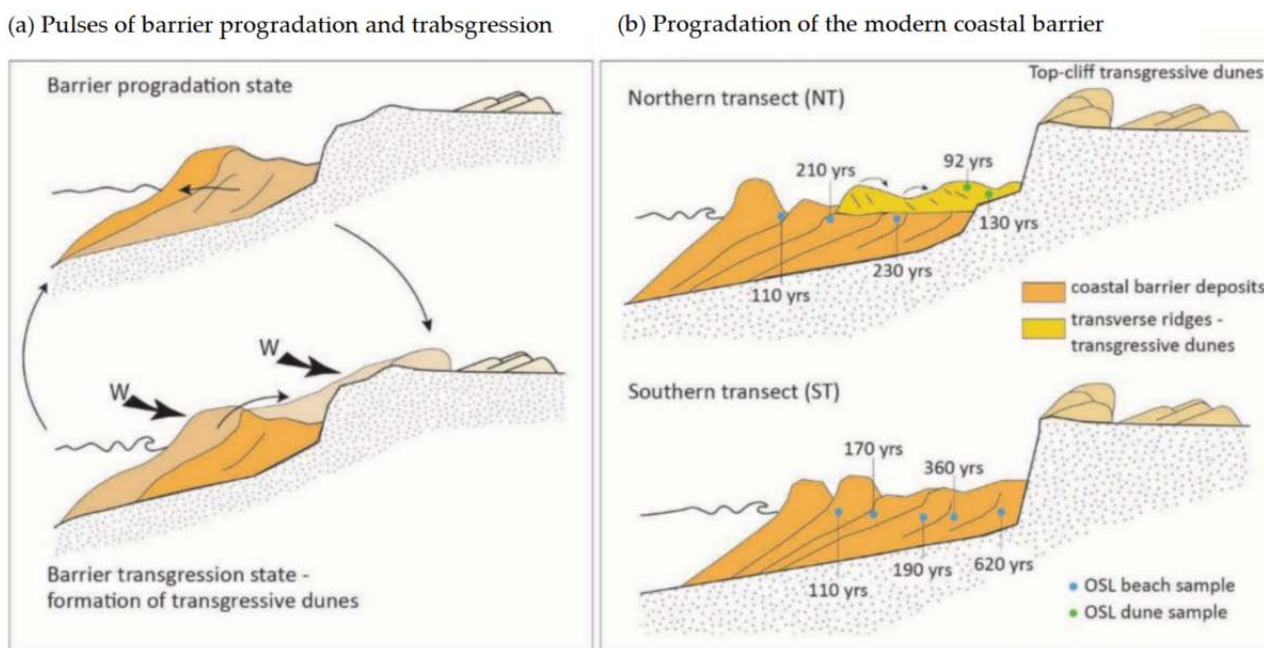


Figure 7. Panel (a) represents the states that the coastal barrier appears to display, alternating between a progradation state with seaward growth of the barrier, a transgressive state with a retreat of the coastline, the dismantling of the barrier and the transference of a part of the sand that eroded from the barrier to the transgressive dunes. Panel (b) represents the last pulse of barrier progradation documented by the collected stratigraphy and dates.

Dune samples suggest that the mobile dune was active at least between 130 and 76 years ago. These ages also suggest that the dunes were active when the coastal barrier dimensions (barrier width) were close to the present ones, and progradation rates were relatively high (i.e., 1.64 m/year in transect NT and 0.65 m/year in transect ST). Interestingly, this period of rapid progradation occurred after the impact of the tsunami associated with the Lisbon Earthquake in 1755.

Previous investigations suggested that the transgressive dune field, developed at the top of the adjacent cliff, derived from the dismantling of former coastal barriers through the landward migration of at least two pulses of transgressive dunes occurring around 5.6 and 1.2–0.98 ka ago [16]. This implies the partial or complete destruction of a former barrier while transgressive dunes were forming (Figure 7a). In this regard, the results presented here support the destruction of former barriers and the growth of a new one at the toe of the eroded cliff. Thus, the results are compatible with the complete destruction of a former barrier during transgression and the formation of new barriers, such as the modern one, which represents, as for Segment A (see Section 2.1), the latest pulse of barrier progradation, occurring after 620 years ago (Figure 7b).

4.2. Comparing the Coastal Barriers

The three selected coastal barriers presented different evolutionary histories and subsurface stratigraphy. The main differences between the evaluated systems were the ages of the modern barriers, the variety of facies within the subsurface stratigraphy, the occurrence of transgressive dune fields and their position relative to the modern coastal barriers. The number of facies identified within each barrier appears related to the variety of configurations identified within the upper part of the subsurface images. The latter appears mostly linked to the type of dunes that can be found within each system, i.e., (i) foredunes defined as shore-parallel ridges formed on top of the backshore [46],

(ii) blowouts resulting from the erosion and fragmentation of former foredunes, (iii) parabolic dunes associated with the migration of blowouts, (iv) transgressive dune fields formed by transverse or barchanoid ridges, and (v) coalescent or nested parabolic dunes, forming transgressive dune fields.

4.2.1. Coastal Barriers and Dunes

Foredunes were present in the three studied segments, showing contrasting dimensions and spatial distribution. Segment A presented only one ridge (<12 m above MSL) adjacent to the present coastline and affected by the more recent evolution of the system [17]. Segment B presented a relatively narrow foredune plain with four ridges that disappear to the north where the transgressive dune field modified and recycled former features (see Subaerial morphology Section 4.1.1). Finally, Segment C consisted of a foredune plain with more than ten large ridges with elevations reaching 15 m above MSL [18]. Blowouts and parabolic dunes were common features along Segment C, while neither of the two types of transgressive dune fields was found along this segment.

It is worth noting that the two identified types of transgressive dune fields were active during different time intervals and apparently under different wind directions. Transgressive dune fields represented by nested parabolic dunes formed during several episodes over the second half of the Holocene (5.56 to 0.79 ka) through the inland migration and coalescence of parabolic dunes promoted by onshore (i.e., westerly) winds [16,17]. These were identified within the top-cliff dune field of Segment B and backing the present barrier of Segment A (Figures 2 and 3). The other type of transgressive dunes was represented by transverse ridges oblique to the shoreline (i.e., moving southward and inland), likely promoted by the effect of winds oblique to the coast (i.e., northerlies). The results from the age analysis of these dunes in Segments B and C suggest that they were moving between at least 150 and 76 years ago (Table 2, Figure 5). Thus, aeolian activity within these dunes was contemporary with the growth of the coastal barriers in Segments A and B (Figures 2 and 3). Previous studies suggested that these dunes in Segment A could have started moving earlier, ca. 230 years ago [25], coinciding with the greater progradation rates observed in Segment B.

Overall, the distribution of dune features suggests that foredunes dominate Segment C and that this dune type is associated with more stable or progradational coasts, e.g., [7,47]. On the other hand, transgressive dune fields are common features in Segments A and B. They can form part of the modern coastal barrier or appear detached from it, but in both cases, their formation appears intimately linked to the evolution of the coastal plain. In addition, the type of dune dominating the record or modern morphology, in combination with the trend of the coastal barrier, can be used to define a number of morphological states between the systems that have shifted over time. Identified morphological states can be summarised as the following: State 1, represented by a prograding barrier with foredunes (foredune plain); State 2, featured by a prograding barrier and transverse dune ridges; State 3, represented by a stable to retreating barrier with active blowouts; State 4, characterised by a stable-to-retreating barrier with active parabolic dunes; and State 4, characterised by a transgressive barrier with a transgressive dune field. The onset of the different states at each site over time is represented in Figure 8, which in turn, describes the evolution of each coastal system over time.

4.2.2. Coastal Barrier Ages

The age of the investigated coastal barriers increased to the south, with the northernmost site (i.e., Segment A) yielding an age of around 0.36 ka [17] and the southern one (Segment C) around 6.47 ka [18]. Segment B, located relatively close to Segment C, yielded an age of around 0.62 ka, suggesting an evolutionary history closer to Segment A. Previous hypotheses suggested that both Segment A and B may have gone through several episodes of barrier building and collapse during the Middle to Late Holocene. The latter was inferred from the occurrence of transgressive dune fields inland of the present

coastal barriers, which were interpreted as indicators of barrier erosion [16,17]. If so, it would follow that the present coastal barriers would represent the latest episode of barrier building and stabilisation, while the inland transgressive dune fields would document barrier retrogradation and inland sediment transference through the migration of coalescent parabolic dunes nourished through the dismantling of the former coastal barriers. Conversely, Segment C appears to have been able to preserve the former coastal barrier, which kept growing over time, albeit with varying rates and hiatus in progradation [18]. The occurrence of blowouts and parabolic dunes in this system suggest periods of coastal erosion and retreat (i.e., hiatus in progradation). However, those never led to the formation of any type of transgressive dune field. The occurrence of transgressive dune fields in Segments A and B, concurrently with the latest phase of barrier building, suggests that the direct link between barrier erosion and transgressive dune formation may not apply in all cases [9].

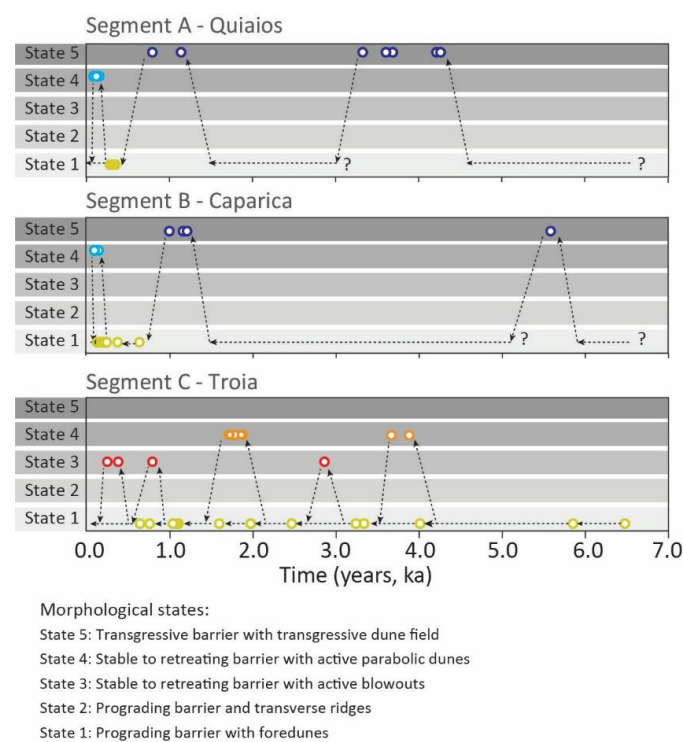


Figure 8. Evolutionary trajectories were reconstructed for each of the three selected study sites. System trajectories result from shifts between morphological states over time. The age of the onset of the different states over time results from the compilation of information from the three selected sites available in [16–18].

5. Discussion

The Portuguese coast has displayed a transgressive trend over the Holocene driven by the eustatic sea-level rise [48]. This trend appears to have been interrupted by the attenuation of the sea-level rise rate around 6.0 ka ago with the subsequent development of coastal barriers along the present sandy coastline [21,49]. The analysis of historical maps and archives retrieved from coastal lagoon deposits has led to the conclusion that coastline shaping was mostly controlled by the climatically biased balance between erosion and supply of terrigenous sediments to the shore [48]. However, the lack of information regarding the coastline’s long-term evolution (hundreds to thousands of years) has prevented the identification and comprehension of these balances and the impact of local factors.

The integration of the reconstructed evolution of the three selected sites indicates that coastal barriers along the coast of Portugal have displayed different evolutionary histories over the Middle to Late Holocene and that the age of modern coastal barriers can vary from thousands to hundreds of years. In addition, the complexity of the explored

sedimentary records suggests non-linear evolutionary trends and barriers shifting between progradation and transgression. Younger ages in the record do not necessarily confirm that these barriers formed within the past hundred years. Instead, they indicate that they may have evolved through a number of pulses that involved the formation of temporary coastal barriers, intercepted by periods of dismantling while moving landward during the Middle to Late Holocene [16,17]. This appears to have been the case for the evolution of the coastal plains in Segments A and B, as suggested by the recent ages of their coastal barriers and the occurrence of fixed transgressive dune fields and lagoon deposits backing them. Conversely, the coastal plain in Segment C shows a single phase of barrier growth, starting around 6.5 ka ago, despite some minor hiatus in progradation.

Fluctuations in the long-term evolution of coastal barrier systems can be described as shifts between morphological states portraying a number of possible paths whose direction is related to the increase or decrease in system stability (Figure 9). Between these two states, additional intermediate states appear to form with different types of dunes within the coastal barrier, defining a spectrum of states that may coexist alongshore as a result of spatial organisation. It is likely that other states may exist; However, the limited record prevents their identification. In addition, it is key to highlight that multiple states may coexist within a system through a spatial organisation, as coastal barriers can be defined as multistable dynamical systems [50]. Therefore, shifts between states or the presence of intermediate states can be used to define the system’s evolutionary trajectories (Figure 8), pin-pointing the response of the system (i.e., perturbation) to changes in drivers or controlling variables (i.e., disturbances). For example, the presence of blowouts represents the response of the foredune system to an internal or external disturbance. If the disturbance relaxes (i.e., pulse disturbance [51]), the system may return to the foredune state, sealing the blowout. However, if the disturbance is maintained or increases in strength with time (i.e., ramp disturbance [52]), one would expect the multiplication of blowouts that may eventually become parabolic dunes and, ultimately, transgressive dunes. The latter may happen if the disturbance, due to either magnitude and/or persistence, causes the system to collapse and enter a phase of reorganisation that lasts until a new position is found and a new barrier can be built. This can be linked to system resilience [53], considering such morphological changes as state shifts in response to press/ramp disturbances. Such disturbances can force the system to a tipping point or threshold that, once crossed, the system can no longer adapt under its current organisation but, instead, needs to reorganise to cope with disturbances. In the particular case of Segments A and B, the record only preserves state end-members (i.e., transgressive dune field, foredune plain), which does not rule out the existence of intermediate states during the evolution trajectories (Figure 8).

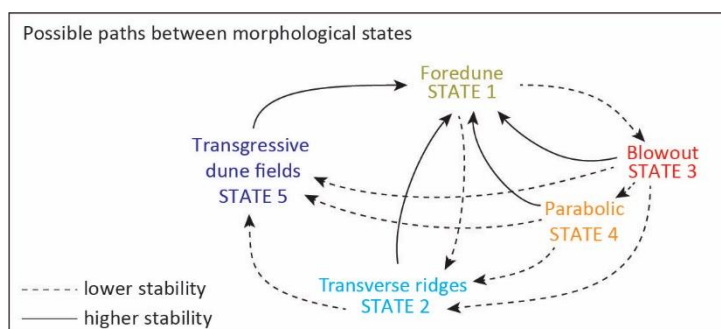


Figure 9. Diagram showing possible fluctuations or shifts between system states defined by the type of dunes (i.e., varying from fixed or foredunes to mobile transgressive dune fields). The arrows represent the possible paths between states, implying an increase or decrease in system stability. State 1 represents a prograding barrier with foredune(s), State 2 is a prograding barrier with transverse ridges, State 3 corresponds to a stable-to-retreating barrier with active blowouts, State 4 is a stable-to-retreating barrier with active parabolic dunes, and State 5 represents a transgressive barrier with a transgressive dune field.

The three selected systems are among the largest along the Portuguese coast in terms of spatial dimensions and sediment budget, and they are relatively close in terms of spatial distribution. Nevertheless, contrasting evolution histories raise questions regarding (i) why these systems have displayed such different trajectories and states over time, (ii) whether these changes simultaneously occurred or not in all three systems, and (iii) what is/are the main source(s) of system disturbance. The selected sites represent key examples to explore the main drivers of change in the long-term evolution of coastal barriers, the onset of state shifts and the potential identification of system state thresholds. To answer these questions, the possible impact of different system characteristics and drivers, including wave and wind exposure and climate variability, will be examined in relation to the evolution of the three sites.

5.1. Drivers of Spatial Variability

The main difference between the studied sites in terms of evolution is related to different ranges in state shifts, reducing severity (i.e., the morphological difference between states) to the south. In this regard, the extremes in the spectrum of states varied between sites, with systems in Segment A and B ranging between “prograding barrier with foredunes” to “transgressive barrier with transgressive dune field”. In contrast, system variability in Segment C ranged between “prograding barrier with foredunes” to “stable to retreating barrier with active parabolic dunes”. Assuming that the three systems should share a similar behaviour as the same components form them, different ranges in system responses or perturbances suggests a range in the magnitude of the exerted disturbance, likely related to site-specific characteristics that translate to varying abilities to absorb disturbances for each system.

In this regard, a critical difference between the three sites is the relation of the coastal configuration relative to the incidence of waves and winds, with different degrees of sheltering due to inherited irregularities in the coastal landscape. Regarding exposure to waves, on the one hand, it has been found that wave energy potential decreases to the south, with annual averages ranging from 200 MWh m^{-1} on the northern coast to 150 MWh m^{-1} on the southwest coast [54]. On the other hand, the orientation of the coastline relative to the wave angle approach plays a major role in determining the potential energy that reaches the coast. The effect of refraction on dissipating wave energy is higher in sections least orientated with the annual average wave direction, leading to a higher energy reduction along those coastal areas [54]. Segment A is located in the most energetic part of the coast of the Portuguese continental coast, facing incident waves almost perpendicularly and without significant obstacles to wave propagation. The latter explains the straight (i.e., drift-aligned) morphology of this dynamic and energetic coastline dominated by strong longshore sediment transport. Conversely, Segments B and C are located behind prominent headlands, which appear responsible for the curvature of the coastline (i.e., swash-aligned) and the reduction in wave exposure. Following the criteria suggested by Klein and Menezes [55], the degree of coastline exposure can be qualitatively assessed by applying embayment scaling parameters [56,57], namely, the indentation ratio (ratio of bay indentation to headland spacing) and the wave obliquity (angle between the shoreline of the downdrift section of the bay and the headland alignment). The embayment parameterization of Segments B and C suggests that the beaches are mostly exposed to waves approaching from angles below 306° N (i.e., obliquity values below 40°), while they are semi-exposed or sheltered to northern waves. This implies that these segments are directly exposed to only 35% of the approaching waves and that dominant waves in the region appear to be largely modified and reduced before reaching the coast. Indentation ratios are greater at Segment C (i.e., 0.48) than at Segment B (i.e., 0.30), which may also imply a more stable coast due to a deeper embayment configuration. The above suggests that the three sites receive very contrasting levels of wave energy, significantly decreasing from the northern Segment A (totally exposed) to the southern Segment C (sheltered) because of the combined effect of latitudinal location and sheltering provided by prominent headlands.

This spatial difference may, in turn, translate into a gradient from a very unstable coast in the north to a very stable coast in the south. In terms of wind incidence, the comparison of offshore (SIMAR re-analysis grid points) wind velocities along the explored coast suggest a reduction in the intensity of the wind toward the south, reaching up to 40% of wind velocity reduction between Segment A and C. It is important to note that Segment C, the segment with no transgressive dune occurrence, is protected by the Arrabida Mountain, which has a maximum elevation of 501 m above MSL and affects the local winds by deflecting northerlies toward the west [58]. Thus, Segment C appears highly protected from the direct impact of both dominant waves and winds, which in turn explains its greater stability and record preservation. Conversely, Segment A is directly exposed to both dominant winds and waves, presenting a greater dynamism and low potential for record preservation. However, differences in wave and wind exposure among the three sites cannot easily explain the fluctuating behaviour displayed by Segments A and B.

In this regard, it is also critical to consider the factors controlling the long-term sediment budget in each site. Most of the sediment within the examined coastal systems could have resulted from the recycling of a finite volume of sediment incorporated into the active coastal zone through marine transgression, despite small losses and inputs from contemporary rivers and longshore sediment transport. It is hypothesised that this volume of sediment has predominantly derived from the reworking of shelf sands and locally from the erosion of bluffs of unconsolidated sediments (e.g., a large part of the cliff backing Segment B consists of semi-consolidated river sands). This is compatible with the occurrence of coastal transgressive dune fields formed during the Late Pleistocene [15,59] after the aeolian reactivation of the sediment-rich subaerial shelf. Therefore, examined segments may have had a finite volume of sediment, which could theoretically have remained stable, or increased or decreased depending on (i) longshore sediment exchanges with adjacent coastal segments, (ii) cross-shore losses, and/or (iii) inland sediment transference through the migration of transgressive dune fields. Following this, one would expect a greater reduction in the local sediment stock over time from Segment C to Segment A, linked to the greater dynamism of the more exposed coastline. In this regard, documented shifts between morphological states (i.e., prograding coastal barrier and inland migrating transgressive dunes) could have been triggered by the onset of a negative sediment budget, whose severity might be directly linked to wave exposure, and reflects the impact of site characteristics on long-term morphological trends. If so, the reconstructed system evolution trajectories could be explained without reference to additional shifts in external forces but solely to self-organising processes. Self-organisation appears to be a common property of geomorphic environments that are characterised by interactions between hydrodynamics and sediment [60], providing simple and alternative explanations for the development of complex behaviours, e.g., [61,62].

5.2. Drivers State Shifts at Regional Scale

As aforementioned, the evaluated sites have gone through a series of fluctuations that implied shifts between morphological states. Whether fluctuations have simultaneously occurred at the evaluated sites is not an easy question to answer due to the preservation of the record and the number of samples dated. Despite these limitations, some general trends can be drawn from the available information that suggests the simultaneous occurrence of shifts across systems. The preserved recorded and dated samples document that the onset of the morphological state of transgressive barrier with transgressive dune field appears to have occurred around 5.6 ka in Segment B and around 4.3 to 3.3 ka in Segment A. During this time interval, large parabolic dunes formed in Segment C, suggesting a relative instability in this coastal segment during this period. A new episode of barrier dismantling and inland migration of transgressive dune fields were recorded between 1.15 and 0.79 ka at both Segments A and B, while Segment C recorded the formation of blowouts. This apparent simultaneity in the occurrence of state shifts across sites suggests that exter-

nal, regional-scale disturbances (i.e., climate-related factors) must have a role in the onset of these shifts.

Previous works linked the occurrence of minor transgressions and regressions [48] to changes in river discharges and associated sediment supply to the coast induced by fluctuations in precipitation regimes. The contribution of rivers has been traditionally used to explain the growth and maintenance of coastal barriers along the northern coast of Portugal [63]. However, this contribution has never been properly assessed, being inferred from historical maps, aerial photographs and volumes of dredged sediment [64]. Results from recent monitoring work in two estuaries of the northern coast support that rivers can only export fine sediments under intense flooding conditions [65]. Fine sediments are ultimately accumulated as mud patches within the inner shelf [66,67] but do not contribute to nourishing the adjacent coastline [65].

Alternatively, the occurrence of state shifts has been tentatively related to climate-related changes in wave and wind regimes, and in particular to changes in storminess activity [16,17], building on the principle that beach morphology is coupled to hydrodynamic processes through sediment transport [68]. The shift to a transgressive barrier state coincides with strong aeolian activity (i.e., formation of transgressive dune fields) around 5.6, 4.2 and 1.15 ka, which has been related to the onset of intense and frequent westerly winds [16,17]. Costas et al. [15] demonstrated that present windfield regimes in southern Europe could not explain past aeolian activity and suggested alternative atmospheric configurations that could have generated aeolian events of such magnitude, including southward diversion of the jet stream, the North Atlantic westerlies and the storm-tracks, very deep cyclones at mid-latitudes over the Atlantic, persistently low-to-negative NAO-like patterns and Arctic amplification (i.e., the poles cooled more strongly than the Tropics). These configurations appear to be compatible with the occurrence of rapid climate change events of global representation identified by Mayewski et al. [69] and the North Atlantic cooling events identified by Bond et al. [70,71]. These events described the large-scale climate variability during the Holocene and were characterised by cool poles, dry tropics and stronger westerlies over the North Atlantic.

Additional research supports millennial to centennial shifts in the latitudinal position of North Atlantic westerlies and storm tracks during the Holocene [72,73], induced by changes in the position and strength of the Azores High pressure system and of the polar vortex. These works found a good correlation between North Atlantic cooling events and storminess activity at higher latitudes and suggested a seesaw pattern between northern and southern Europe, resembling the present-day NAO variability. This would imply, for example, lower storm activity across southwestern Europe and northwestern Africa (i.e., the southern region of the temperature dipole that characterises the NAO pattern) during positive NAO-like conditions, e.g., [74,75].

Alternatively, good correspondence was found between most North Atlantic cooling events and enhanced precipitation [76,77], which the authors interpreted as indicative of prevailing negative NAO-like conditions. In this line, Taylor et al. [78] found changes in moisture transport trajectories (i.e., from tropical or high-latitude regions) during the Holocene that suggest a stronger polar climatic influence on the Portuguese coast and much of Europe during cooling events. The latter would represent a scenario characterised by an intensification of westerly zonal winds resulting from a stronger latitudinal temperature gradient across the Atlantic and a southward displacement and deepening of the Icelandic low. This mechanism would explain enhanced westerly winds and storm tracks along the entirety of the European coastline in combination with the southward extension of polar moisture transport, in line with Costas et al. [15,16], presenting an alternative to the seesaw pattern.

The above alternative scenarios and mechanisms reflect the current debate surrounding the Holocene climate in the North Atlantic [76,79,80], including the pattern of storminess distribution during these events in southwestern Europe and northern Africa. In addition, it is important to stress that the lack of regional coherence might also be linked to additional

factors, such as local conditions and type of proxy, which may affect the record and obscure the regional climate signal [77]. Nevertheless, most documented environmental reconstructions clearly demonstrate that millennial-scale cycles dominated the climate variability during the Holocene and could have had a great impact on modulating the evolution of the sandy coast of Portugal, particularly along the zones largely exposed to wave climate and its variability.

6. Conclusions

The present work follows previous research focusing on reconstructing the Middle to Late Holocene evolution of three coastal barriers located along the western Portuguese coast. Barrier evolution was reconstructed by combining information on the internal architecture of the studied sites obtained using a GPR, the morphology of the modern barrier and the age of selected beach and dune depositional units using OSL. The sites present different configurations that result from inherited coastal morphology, which ultimately controls the exposure to waves and winds, increasing from the highly protected southern site to the northern one, which directly faces open ocean waves.

The results document contrasting evolutionary histories defined by fluctuations or shifts between a range of identified morphological states at each site. Contrasting trajectories displayed by each site explain the different ages of the modern systems, with two of the sites displaying very young ages (i.e., 360 and 620 years) compared to the third one (i.e., 6.47 ka). The former cases are located along the more energetic and exposed coast, particularly the youngest barrier, while the third corresponds to the highly sheltered site. The younger ages of the barriers, together with the presence of several pulses of inland migration of transgressive dunes (dated around 5.6, 4.3 to 3.3 and 1.15 ka), were interpreted as indicative of the onset of phases of barrier instability and dismantling (transgressive barrier with a transgressive dune field state). These instability phases appear to have alternated with phases of stability and growth (prograding barrier with foredune(s) state) over time within a trend of coastline retreat. Conversely, the third case shows a single phase of barrier stability and growth (prograding barrier with foredune(s) state), despite some minor hiatus in progradation represented by the occurrence of blowouts (stable to retreating barrier with blowouts state) and parabolic dunes (stable to retreating barrier with parabolic dunes state). An additional morphological state was identified within the northern and more unstable sites, represented by a prograding barrier with a transgressive dune field formed by transverse ridges. In relation to the differences in the trajectories of the three sites, the main difference is the range of states that the systems appear to adopt while reorganising to cope with disturbances. In this regard, the northern exposed sites displayed a greater range of states whose extremes were marked by two morphological end-members: progradational and transgressive barriers, with the first related to a high degree of stability and the second to the lowest degree of system stability. Intermediate states (e.g., barrier with blowouts) may have developed between these two extremes; However, the low preservation of the record at these sites prevents the elaboration of more detailed system trajectories. The sheltered southern site displayed a smaller range of states limited to shifts between the stable state (prograding barrier) and intermediate unstable states, such as the barrier with blowouts and parabolic dunes. This suggests that highly dynamic exposed areas present a lower capacity to absorb a disturbance, which could be explained by a greater magnitude of the exerted disturbance in these areas or by their inherent greater fragility. The latter seems associated with a higher tendency to system instability likely linked to local unbalanced longshore sediment transport locally. In addition, the results suggest that system state shifts appear to have simultaneously occurred across the studied sites, pointing to regional scale factors impacting the systems at the centennial to millennial temporal scale. These factors appear related to Holocene climate variability and, in particular, to the onset of storminess activity at the regional scale.

Finally, it is worth highlighting that the areas with a lower capacity to absorb disturbances and where instability appears to happen more often with greater consequences in

terms of system reorganisation at a long-term temporal scale coincide with areas that are currently suffering severe problems of erosion and coastline retreat. The latter suggests that despite being induced by very different causes (e.g., the current situation has been related to human-related activities), the current erosion problems reflect the fragility of the system and its high tendency to enter instability, which may increase over time, threatening the future existence of these systems.

Funding: This research was funded by Fundação para a Ciência e a Tecnologia (FCT), grant number PTDC/CTE-GIX/101466/2008. The author recognises the support of national funds through FCT under the project LA/P/0069/2020, granted by the Associate Laboratory ARNET, and UID/00350/2020 CIMA. The author was supported by the contract 2021.04286.CEECIND, funded by FCT.

Data Availability Statement: Data will be made available on request.

Acknowledgments: The author would like to thank Katerina Kombiadou for her comments and suggestions to improve the manuscript structure. Thanks are also given to Ronald Goble for his careful work dating the dune and beach samples and to all the people who helped in the fieldwork during this project's progress.

Conflicts of Interest: The author declares no conflict of interest.

References

1. Fitzgerald, D.M.; Buynevich, I. Coastal Barriers. In *Coastal Zones and Estuaries*; Isla, F.I., Ed.; EOLSS Publishers Co Ltd: Oxford, UK, 2009; pp. 164–189.
2. Kraft, J.C.; John, C.J. Lateral and Vertical Facies Relations of Transgressive Barrier. *AAPG Bulletin* **1979**, *63*, 2145–2163.
3. Thom, B.G. Transgressive and regressive stratigraphies of coastal sand barriers in southeast Australia. *Mar. Geol.* **1984**, *56*, 137–158. [[CrossRef](#)]
4. Morton, R.A. Texas Barriers. In *Geology of Holocene Barrier Island Systems*; Davis, R.A., Ed.; Springer: Berlin/Heidelberg, Germany, 1994; pp. 75–114.
5. Dillenburg, S.R.; Barboza, E.G.; Tomazelli, L.J.; Rosa, M.L.C.C.; Maciel, G.S. Aeolian Deposition and Barrier Stratigraphy of the Transition Region between a Regressive and a Transgressive Barrier: An example from Southern Brazil. *J. Coast. Res.* **2013**, *65*, 464–469. [[CrossRef](#)]
6. Forbes, D.L.; Orford, J.D.; Carter, R.W.G.; Shaw, J.; Jennings, S.C. Morphodynamic evolution, self-organisation, and instability of coarse-clastic barriers on paraglacial coasts. *Mar. Geol.* **1995**, *126*, 63–85. [[CrossRef](#)]
7. Psuty, N.P. The Coastal Fore-dune: A Morphological Basis for Regional Coastal Dune Development. In *Coastal Dunes. Ecological Studies*; Martínez, M.L., Psuty, N.P., Eds.; Springer-Verlag: Berlin, Germany, 2004; pp. 11–27.
8. Hesp, P. Conceptual models of the evolution of transgressive dune field systems. *Geomorphology* **2013**, *199*, 138–149. [[CrossRef](#)]
9. Hesp, P.A.; DaSilva, M.; Miot da Silva, G.; Bruce, D.; Keane, R. Review and direct evidence of transgressive aeolian sand sheet and dunefield initiation. *Earth Surf. Process. Landforms* **2022**, *47*, 2660–2675. [[CrossRef](#)]
10. Pye, K. Models of transgressive coastal dune building episodes and their relationship to Quaternary sea level changes: A discussion with reference from eastern Australia. In *Coastal Research: UK Perspectives*; Clark, M., Ed.; Workshop of the Small Study Group on Nearshore Dynamics: Norwich, UK, 1984; pp. 81–104.
11. Thom, B.G. Coastal erosion in eastern Australia. *Search* **1974**, *5*, 198–209. [[CrossRef](#)]
12. Armitage, S.J.; Botha, G.A.; Duller, G.A.T.; Wintle, A.G.; Rebêlo, L.P.; Momade, F.J. The formation and evolution of the barrier islands of Inhaca and Bazaruto, Mozambique. *Geomorphology* **2006**, *82*, 295–308. [[CrossRef](#)]
13. Andreucci, S.; Clemmensen, L.B.; Pascucci, V. Transgressive dune formation along a cliffed coast at 75 ka in Sardinia, Western Mediterranean: A record of sea-level fall and increased windiness. *Terra Nov.* **2010**, *22*, 424–433. [[CrossRef](#)]
14. Ponte Lira, C.; Nobre Silva, A.; Taborda, R.; Freire de Andrade, C. Coastline evolution of Portuguese low-lying sandy coast in the last 50 years: An integrated approach. *Earth Syst. Sci. Data* **2016**, *8*, 265–278. [[CrossRef](#)]
15. Costas, S.; Naughton, F.; Goble, R.; Renssen, H. Windiness spells in SW Europe since the last glacial maximum. *Earth Planet. Sci. Lett.* **2016**, *436*, 82–92. [[CrossRef](#)]
16. Costas, S.; Jerez, S.; Trigo, R.; Goble, R.; Rebêlo, L. Sand invasion along the Portuguese coast forced by westerly shifts during cold climate events. *Quat. Sci. Rev.* **2012**, *42*, 15–28. [[CrossRef](#)]
17. Costas, S.; Brito, P.; FitzGerald, D.; Goble, R. Climate-driven episodes of dune mobilization and barrier growth along the central coast of Portugal. *Geol. Soc. London, Spec. Publ.* **2013**, *388*, 407–427. [[CrossRef](#)]
18. Costas, S.; Rebêlo, L.; Brito, P.; Burbidge, C.; Prudêncio, M.; FitzGerald, D. The Joint History of Tróia Peninsula and Sado Ebb-Delta. In *Sand and Gravel Spits*; Randazzo, G., Jackson, D.W.T., Cooper, J.A.G., Eds.; Springer International Publishing: Berlin/Heidelberg, Germany, 2015; Volume 12, pp. 79–102; ISBN 978-3-319-13715-5.
19. Costa, M.; Silva, R.; Vitorino, J. Contribuição para o estudo do clima de agitação marítima na costa Portuguesa. In Proceedings of the II Jornadas Portuguesas de Engenharia Costeira e Portuária, Sines, Portugal, 17–19 October 2001.

20. Silva, A.N.; Taborda, R.; Bertin, X.; Dodet, G. Seasonal to Decadal Variability of Longshore Sand Transport at the Northwest Coast of Portugal. *J. Waterw. Port Coast. Ocean. Eng.* **2012**, *138*, 464–472. [[CrossRef](#)]
21. Costas, S.; Ferreira, O.; Plomaritis, T.A.; Leorri, E. Coastal barrier stratigraphy for Holocene high-resolution sea-level reconstruction. *Sci. Rep.* **2016**, *6*, 38726. [[CrossRef](#)]
22. Menezes, G. *Estudo da evolução da linha de costa entre o cabo Mondego e Aveiro (1958–2010)*; Universidade de Coimbra: Coimbra, Portugal, 2011.
23. Bernardes, C.; Rocha, F. Temporal evolution of the sand-spit between Torreira and Furadouro (NW Portugal). *J. Coast. Res.* **2007**, *2007*, 1092–1096.
24. Danielsen, R.; Castilho, A.M.; Dinis, P.A.; Almeida, A.C.; Callapez, P.M. Holocene interplay between a dune field and coastal lakes in the Quiaios-Tocha region, central littoral Portugal. *Holocene* **2012**, *22*, 383–395. [[CrossRef](#)]
25. Clarke, M.L.; Rendell, H.M. Effects of storminess, sand supply and the North Atlantic Oscillation on sand invasion and coastal dune accretion in western Portugal. *Holocene* **2006**, *16*, 341–355. [[CrossRef](#)]
26. Azevedo, M.T. O sinclinal de Albufeira, Evolução pós miocénica e reconstrução paleogeográfica. Ph.D. Thesis, Universidade de Lisboa, Lisboa, Portugal, 1983.
27. Palma, M.; Dias, J.A.; Freitas, J.G. It's not only the sea: A history of human intervention in the beach-dune ecosystem of Costa da Caparica (Portugal). *J. Integr. Coast. Zo. Manag.* **2021**, *21*, 227–247. [[CrossRef](#)]
28. Antunes, M.T.; Pais, J. Paisagem protegida da Arriba Fossil da Caparica. *Lib. Bol. da Liga para a Proteção da Nat.* **1992**, *42*, 5–9.
29. Jacob, J.; Gama, C.; Liu, J.; Silva, A. Shadowing effects on beach morphodynamics during storm events on Tróia-Sines embayed coast, southwest Portugal. *J. Coast. Res.* **2009**, *1*, 73–77.
30. Daniels, D.J. Ground Penetrating Radar. In *Encyclopedia of RF and Microwave Engineering*; Daniels, D.J., Ed.; John Wiley & Sons, Inc.: Hoboken, NJ, USA, 2005; ISBN 9780471654506.
31. Méndez, G.; Pérez-Arlucea, M.; Stouthammer, E.; Berensden, H. The TESS-1 suction corer: A new device to extract wet, uncompacted sediments. *J. Sediment. Res.* **2003**, *73*, 1078–1081. [[CrossRef](#)]
32. Aitken, M.J. *An Introduction to Optical Dating. The Dating of Quaternary Sediments by the Use of Photon-Stimulated Luminescence*; Oxford University Press: New York, NY, USA, 1998.
33. Adamiec, G.; Aitken, M. Dose-rate conversion factors: Update. *Anc. TL* **1998**, *16*, 37–50.
34. Guerin, G.; Mercier, N.; Adamiec, G. Dose-rate conversion factors: Update. *Anc. TL* **2011**, *29*, 5–8.
35. Brennan, B.J. Beta doses to spherical grains. *Radiat. Meas.* **2003**, *37*, 299–303. [[CrossRef](#)]
36. Prescott, J.R.; Hutton, J.T. Cosmic ray contributions to dose rates for luminescence and ESR dating: Large depths and long-term time variations. *Radiat. Meas.* **1994**, *23*, 497–500. [[CrossRef](#)]
37. Murray, A.S.; Wintle, A.G. Luminescence dating of quartz using an improved single-aliquot regenerative-dose protocol. *Radiat. Meas.* **2000**, *32*, 57–73. [[CrossRef](#)]
38. Galbraith, R.F.; Roberts, R.G.; Laslett, G.M.; Yoshida, H.; Olley, J.M. Optical dating of single and multiple grains of quartz from Jinnium Rock Shelter, Northern Australia: Part I, experimental design and statistical models. *Archaeometry* **1999**, *41*, 339–364. [[CrossRef](#)]
39. Rodnight, H. How many equivalent dose values are needed to obtain a reproducible distribution? *Anc. TL* **2008**, *26*, 3–9.
40. Durcan, J.A.; Duller, G.A.T. The fast ratio: A rapid measure for testing the dominance of the fast component in the initial OSL signal from quartz. *Radiat. Meas.* **2011**, *46*, 1065–1072. [[CrossRef](#)]
41. Bailey, R.M.; Arnold, L.J. Statistical modeling of single grain quartz De distributions and an assessment of procedures for estimating burial dose. *Quat. Sci. Rev.* **2006**, *25*, 2475–2502. [[CrossRef](#)]
42. Pilar, P.; Soares, C.G.; Carretero, J.C. 44-year wave hindcast for the North East Atlantic European coast. *Coast. Eng.* **2008**, *55*, 861–871. [[CrossRef](#)]
43. Mitchum, J.R.M.; Vail, P.R.; Sangree, J.B. Seismic stratigraphy and global changes of sea level-Part 6: Stratigraphic interpretation of seismic reflection patterns in depositional sequences. In *Seismic Stratigraphy-Applications to Hydrocarbon Exploration*; Payton, C.E., Ed.; American Association of Petroleum Geologists: Tulsa, OK, USA, 1977; pp. 117–133.
44. Van Heteren, S.; Fitzgerald, D.M.; McKinlay, P.A.; Buynevich, I.V.; van Heteren, S.; Fitzgerald, D.M.; McKinlay, P.A.; Buynevich, I. V Radar facies of paraglacial barrier systems: Coastal New England, USA. *Sedimentology* **1998**, *45*, 181–200. [[CrossRef](#)]
45. Costas, S.; Alejo, I.; Rial, F.; Lorenzo, H.; Nombela, M.A. Cyclical evolution of a modern transgressive sand barrier in northwestern Spain elucidated by GPR and aerial photos. *J. Sediment. Res.* **2006**, *76*, 1077–1092. [[CrossRef](#)]
46. Hesp, P. Foredunes and blowouts: Initiation, geomorphology and dynamics. *Geomorphology* **2002**, *48*, 245–268. [[CrossRef](#)]
47. Herrero, X.; Costas, S.; Kombiadou, K. Coastal ridge constructive processes at a multi-decadal scale in Barreta Island (southern Portugal). *Earth Surf. Process. Landforms* **2020**, *45*, 411–423. [[CrossRef](#)]
48. Dias, J.M.A.; Boski, T.; Rodrigues, A.; Magalhães, F. Coast line evolution in Portugal since the Last Glacial Maximum until present—A synthesis. *Mar. Geol.* **2000**, *170*, 177–186. [[CrossRef](#)]
49. Freitas, M.D.C.; Andrade, C.; Rocha, F.; Tassinari, C.; Munhá, J.M.; Cruces, A.; Vidinha, J.; Da Silva, C.M.; Freitas, M.C.; Andrade, C.; et al. Lateglacial and Holocene environmental changes in Portuguese coastal lagoons 1: The sedimentological and geochemical records of the Santo André coastal area. *Holocene* **2003**, *13*, 433–446. [[CrossRef](#)]
50. Zinnert, J.C.; Stallins, J.A.; Brantley, S.T.; Young, D.R. Crossing Scales: The Complexity of Barrier-Island Processes for Predicting Future Change. *Bioscience* **2017**, *67*, 39–52. [[CrossRef](#)]

51. Bender, E.A.; Case, T.J.; Gilpin, M.E. Perturbation Experiments in Community Ecology: Theory and Practice. *Ecology* **1984**, *65*, 1–13. [[CrossRef](#)]
52. Lake, P.S. Disturbance, patchiness, and diversity in streams. *J. N. Am. Benthol. Soc.* **2000**, *19*, 573–592. [[CrossRef](#)]
53. Piégay, H.; Chabot, A.; Le Lay, Y.-F. Some comments about resilience: From cyclicity to trajectory, a shift in living and nonliving system theory. *Geomorphology* **2020**, *367*, 106527. [[CrossRef](#)]
54. Mota, P.; Pinto, J.P. Wave energy potential along the western Portuguese coast. *Renew. Energy* **2014**, *71*, 8–17. [[CrossRef](#)]
55. da Fontoura Klein, A.H.; de Menezes, J.T. Beach Morphodynamics and Profile Sequence for a Headland Bay Coast. *J. Coast. Res.* **2001**, *17*, 812–835.
56. Silvester, R.; Hsu, J.R.C. *Coastal Stabilization*; World Scientific: Singapore, 1997; Volume 14; ISBN 978-981-02-3137-8.
57. Silvester, R.; Hsu, J.R.C. *Coastal Stabilization: Innovative Concepts*; Prentice-Hall, Inc.: Englewood Cliffs, NJ, USA, 1993.
58. Neto, C.S. A circulação do ar na Península de Tróia e na Costa da Galé. *Finisterra Rev. Port. Geogr.* **2000**, *35*, 41–55.
59. Granja, H.M.; Groot, T.A.M.D.; Costa, A.L. Evidence for Pleistocene wet aeolian dune and interdune accumulation, S. Pedro da Maceda, north-west Portugal. *Sedimentology* **2008**, *55*, 1203–1226. [[CrossRef](#)]
60. Coco, G.; Murray, A.B. Patterns in the sand: From forcing templates to self-organization. *Geomorphology* **2007**, *91*, 271–290. [[CrossRef](#)]
61. Plant, N.G.; Freilich, M.H.; Holman, R.A. Role of morphologic feedback in surf zone sandbar response. *J. Geophys. Res. Ocean.* **2001**, *106*, 973–989. [[CrossRef](#)]
62. Cooper, J.A.G.; McKenna, J.; Jackson, D.W.T.; O'Connor, M. Mesoscale coastal behavior related to morphological self-adjustment. *Geology* **2007**, *35*, 187–190. [[CrossRef](#)]
63. Taveira-Pinto, F.; Silva, R.; Pais-Barbosa, J. Coastal Erosion Along the Portuguese Northwest Coast Due to Changing Sediment Discharges from Rivers and Climate Change. In *Global Change and Baltic Coastal Zones*; Schernewski, G., Hofstede, J., Neumann, T., Eds.; Springer: Dordrecht, The Netherlands, 2011; Volume 1, pp. 135–151. ISBN 978-94-007-0399-5.
64. Granja, H.M. A geologia do Holocénico aplicada ao ordenamento da zona costeira. *Estud. do Quaternário* **2000**, *3*, 73–90. [[CrossRef](#)]
65. Santos, A.I.; Oliveira, A.; Carinhas, D.; Pinto, J.P.; Freitas, M.C. Hydrodynamic and Sediment Transport Patterns in the Minho and Douro Estuaries (NW Portugal) Based on ADCP Monitoring Data: Part 2—Statistical Interpretation of Bottom Moored Datasets. *Coasts* **2021**, *1*, 56–72. [[CrossRef](#)]
66. Drago, T.; Oliveira, A.; Magalhães, F.; Cascalho, J.; Jouanneau, J.-M.; Vitorino, J. Some evidences of northward fine sediment transport in the northern portuguese continental shelf. *Oceanol. Acta* **1998**, *21*, 223–231. [[CrossRef](#)]
67. Dias, J.M.A.; Jouanneau, J.M.; Gonzalez, R.; Araújo, M.F.; Drago, T.; Garcia, C.; Oliveira, A.; Rodrigues, A.; Vitorino, J.; Weber, O. Present day sedimentary processes on the northern Iberian shelf. *Prog. Oceanogr.* **2002**, *52*, 249–259. [[CrossRef](#)]
68. Aagaard, T.; Greenwood, B.; Hughes, M. Sediment transport on dissipative, intermediate and reflective beaches. *Earth-Science Rev.* **2013**, *124*, 32–50. [[CrossRef](#)]
69. Mayewski, P.A.; Rohling, E.E.; Curt Stager, J.; Karlén, W.; Maasch, K.A.; David Meeker, L.; Meyerson, E.A.; Gasse, F.; van Kreveld, S.; Holmgren, K.; et al. Holocene climate variability. *Quat. Res.* **2004**, *62*, 243–255. [[CrossRef](#)]
70. Bond, G.; Kromer, B.; Beer, J.; Muscheler, R.; Evans, M.N.; Showers, W.; Hoffman, S.; Lotti-Bond, R.; Hajdas, I.; Bonani, G. Persistent solar influence on North Atlantic climate. *Science* **2001**, *294*, 2130–2136. [[CrossRef](#)]
71. Bond, G.; Showers, W.; Cheseby, M.; Lotti, R.; Almasi, P.; DeMenocal, P.; Priore, P.; Cullen, H.; Hajdas, I.; Bonani, G. A pervasive millennial-scale cycle in North Atlantic Holocene and glacial climates. *Science* **1997**, *278*, 1257–1266. [[CrossRef](#)]
72. Goslin, J.; Fruergaard, M.; Sander, L.; Gałka, M.; Menviel, L.; Monkenbusch, J.; Thibault, N.; Clemmensen, L.B. Holocene centennial to millennial shifts in North-Atlantic storminess and ocean dynamics. *Sci. Rep.* **2018**, *8*, 12778. [[CrossRef](#)]
73. Orme, L.C.; Charman, D.J.; Reinhardt, L.; Jones, R.T.; Mitchell, F.J.G.; Stefanini, B.S.; Barkwith, A.; Ellis, M.A.; Grosvenor, M. Past changes in the North Atlantic storm track driven by insolation and sea-ice forcing. *Geology* **2017**, *45*, 335–338. [[CrossRef](#)]
74. Ramos-Román, M.J.; Jiménez-Moreno, G.; Camuera, J.; García-Alix, A.; Scott Anderson, R.; Jiménez-Espejo, F.J.; Sachse, D.; Toney, J.L.; Carrión, J.S.; Webster, C.; et al. Millennial-scale cyclical environment and climate variability during the Holocene in the western Mediterranean region deduced from a new multi-proxy analysis from the Padul record (Sierra Nevada, Spain). *Glob. Planet. Chang.* **2018**, *168*, 35–53. [[CrossRef](#)]
75. Smith, A.C.; Wynn, P.M.; Barker, P.A.; Leng, M.J.; Noble, S.R.; Tych, W. North Atlantic forcing of moisture delivery to Europe throughout the Holocene. *Sci. Rep.* **2016**, *6*, 24745. [[CrossRef](#)] [[PubMed](#)]
76. Ait Brahim, Y.; Wassenburg, J.A.; Sha, L.; Cruz, F.W.; Deininger, M.; Sifeddine, A.; Bouchaou, L.; Spötl, C.; Edwards, R.L.; Cheng, H. North Atlantic Ice-Rafting, Ocean and Atmospheric Circulation During the Holocene: Insights From Western Mediterranean Speleothems. *Geophys. Res. Lett.* **2019**, *46*, 7614–7623. [[CrossRef](#)]
77. Benson, A.; Hoffmann, D.L.; Daura, J.; Sanz, M.; Rodrigues, F.; Souto, P.; Zilhão, J. A speleothem record from Portugal reveals phases of increased winter precipitation in western Iberia during the Holocene. *Holocene* **2021**, *31*, 1339–1350. [[CrossRef](#)]
78. Taylor, A.K.; Benedetti, M.M.; Haws, J.A.; Lane, C.S. Mid-Holocene Iberian hydroclimate variability and paleoenvironmental change: Molecular and isotopic insights from Praia Rei Cortiço, Portugal. *J. Quat. Sci.* **2018**, *33*, 79–92. [[CrossRef](#)]
79. Sorrel, P.; Debret, M.; Billeaud, I.; Jaccard, S.L.; McManus, J.F.; Tessier, B. Persistent non-solar forcing of Holocene storm dynamics in coastal sedimentary archives. *Nat. Geosci.* **2012**, *5*, 892–896. [[CrossRef](#)]
80. Trouet, V.; Scourse, J.D.; Raible, C.C. North Atlantic storminess and Atlantic Meridional Overturning Circulation during the last Millennium: Reconciling contradictory proxy records of NAO variability. *Glob. Planet. Chang.* **2012**, *84–85*, 48–55. [[CrossRef](#)]